Supplementary Material

TOROIDAL NUCLEI OF COLUMNAR LYOTROPIC CHROMONIC LIQUID CRYSTALS COEXISTING WITH ISOTROPIC PHASE

RUNA KOIZUMI, DMITRY GOLOVATY, ALI ALQARNI, SHAWN W. WALKER, YURIY A. NASTISHIN, M. CARME CALDERER, AND OLEG D. LAVRENTOVICH

S1. Experiment

Interfacial tension. In the past, the surface tension of the C-I interface has been measured for surfactant-based lyotropic phase by the so-called grain boundary groove method [S1], borrowed from metallurgy [S2].

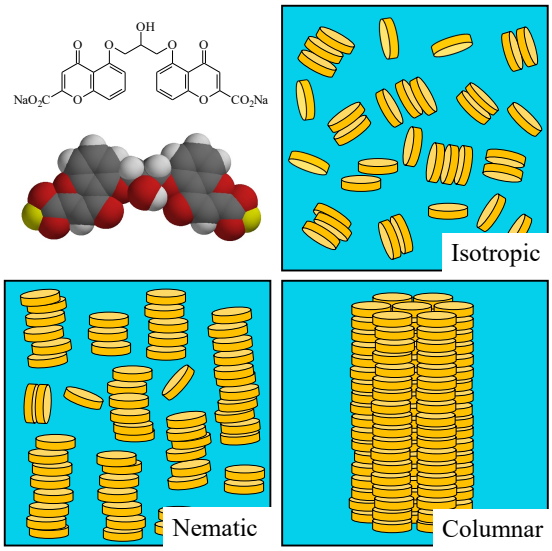

Figure S1. Chemical and space-filling structure of DSCG molecule and molecular arrangements in the isotropic, nematic, and in a filament of a columnar phase. The director $\widehat{\mathbf{n}}$ is along the average alignment direction of the columnar aggregates.

In this approach, one creates a Col-I interface by placing a sample in a temperature gradient and explores the depth h of an indentation caused by the presence of a grain boundary between two domains of the Col phase. If the interface is strictly perpendicular to the temperature gradient, i.e., not curved in the plane normal to the glass plates, the measurement of h yields the surface tension coefficient, $\sigma_{\|} \propto h^2$. Although we do observe an increase of h with c and C, the data could not be used to determine $\sigma_{\|}$ since the Col-I interface makes an angle of about 62°-73° with the glass, as the Col phase wets the substrate better than the I phase. Instead, we use the technique of a spinning drop to determine $\sigma_{\|}$ at the Col-I interface by a spinning droplet technique, which is based on the fact that centrifugal forces acting on a droplet (I phase) placed in a more dense second fluid (Col phase) would elongate. The elongation is limited by the interfacial tension between the two fluids, which allows one to measure the interfacial tension, see [S1, S3, S4, S5, S6] and references therein. The denser fluid (Col phase) fills a round capillary; the droplet of the lighter fluid (I phase) is injected into the central part of the tube. The tube rotates around the symmetry axis with a rotational speed ω. Measuring the thinning diameter δ of the droplet, the interfacial tension is calculated as $\sigma_{\|} = \frac{\delta^3 \omega^2 \Delta\rho}{4}$, where $\Delta\rho$ is the density difference between the two fluids. We centrifuged the $c = 0.47$ mol/kg solution of DSCG

at 4000 rpm at $T = 45^\circ$ C in order to separate the Col and the I phases from each other and measured their densities using a DE45 Density Meter (Mettler Toledo) as $\rho_C = 1.12 \times 10^3$ kg/m^3 and $\rho_I = 1.05 \times 10^3$ kg/m^3, respectively; therefore, $\Delta\rho = 0.07 \times 10^3$ kg/m^3. The interfacial tension is determined by the spinning drop tensiometer DataPhysics Instruments, SVT 20. To enhance contrast between the Col and I phases, the I solution is doped with 0.05 wt% Methylene Blue dye. The measurements of δ at $\omega = 9000$ rpm yield $\sigma \approx 10^{-6}$ J/m^2. Because of high light scattering at the Col phase, more accurate measurements could not be possible.

Bend elastic constant. The independent measurements of K_3 for the Col islands are difficult. Elastic moduli of LCLCs have been measured only for the homogeneous N phase. These measurements suggest that $K_3 \propto \lambda_p c$, where λ_p is the persistence length which could become smaller at higher concentrations c or C since because of the electrostatic effects such as the decrease of the Debye screening length [S7], [S8, S9, S10]. Therefore, the product $\lambda_p c$ and thus K_3 might not increase much with c and C. The estimate of $K_3 = 50$-60 pN based on the fitted value of the elastocapillary length λ_{ec} is slightly larger than the maximum value $K_3 = 50$ pN measured in the homogeneous N phase [S7].

Closure of toroids. The toroidal shapes result from a delicate balance of the anisotropic surface tension and bulk elasticity. The preferred alignment of the director at the Col-I interface is tangential, with a surface tension coefficient $\sigma_\parallel$. This preference is evidenced by parallel alignment of chromonic aggregates at the Col-I interfaces, Figs. 1, S2. Transient perpendicular alignment of **n** at the Col-I interface is observed only when the growing filament are not yet curled into toroids, Fig. S2. The perpendicular alignment is accompanied by a higher surface tension coefficient $\sigma_\perp > \sigma_\parallel$. The two open ends of the filaments in Fig. S2 at t <10 s that are exposed to water carry a surface energy proportional to their surface area $F_{s\perp} = 2\pi a^2 \sigma_\perp$, where we approximate the filament as a circular cylinder of a radius a. The two open ends would tend to come together in order to minimize the exposure of the hydrophobic aromatic cores to water and maximize the exposure of the hydrophilic groups of the DSCG molecules, as clearly seen in Fig. S2 for $t = 60$ s. The toroidal shape is preferred over a filament if the bending energy is smaller than the surface energy $F_{s\perp} = 2\pi a^2 \sigma_\perp$ that the two open ends carry.

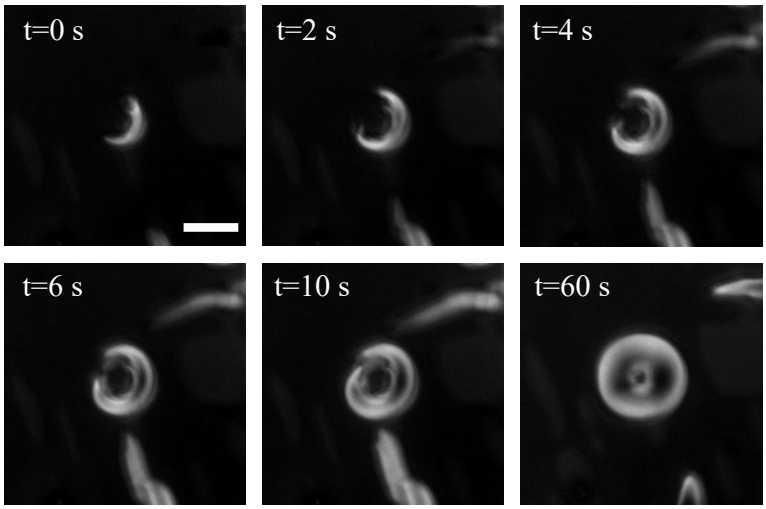

FIGURE S2. Dynamics of the Col toroid formation from bent filaments in the mixture of DSCG, $c = 0.34$ mol/kg (15 wt%), and PEG, $C = 0.016$ mol/kg (5 wt%); $t = 0$ s refers to the time when the cooling rom the isotropic phases was stopped, and the temperature was fixed at $T = 42^\circ$C. Scale bar 50μm.

To calculate the elastic energy of a toroid in Fig. S2, $t = 60$ s, we model it as a circular torus of a minor radius a and a major radius r, associated with the geometrical parameters in Fig. 1d as $r = R - a$, Fig. 1e. The

elastic energy density of bend [S11] is $f_e = \frac{1}{2}K_3(\mathbf{n}\times \mathrm{curl}\mathbf{n})^2$, where K_3 is the bend modulus. We introduce a system of coordinates (ρ,θ,ϕ) related to the Cartesian coordinates and the geometric parameters defined above as

$$\{x,y,z\} = \{(R-a-\rho\cos\theta)\cos\phi, (R-a-\rho\cos\theta)\sin\phi,\ \rho\sin\theta\},$$

Fig. 3a. In these coordinates, $\mathbf{n} = (0,0,1)$ and $(\mathbf{n}\times \mathrm{curl}\mathbf{n})^2 = 1/(R-a-\rho\cos\theta)^2$, the scale factors are $g_{rr} = 1$; $g_{\theta\theta} = \rho^2$; $g_{\phi\phi} = (r-\rho\cos\theta)^2$; the volume element is $dV = \rho(r-\rho\cos\theta)^2$. Integration over $0 \le \rho \le a$; $0 \le \theta,\phi \le 2\pi$ yields the bend energy of the Col torus as $F_e = 2\pi^2 K_3\left(r - \sqrt{r^2-a^2}\right)$. The surface energy of the toroid with tangential director at the Col-I interface is $F_{s\parallel} = 4\pi^2\sigma_\parallel ar$, where $\sigma_\parallel$ is the surface tension coefficient for tangential anchoring at the Col-I interface. The sum $F_e + F_{s\parallel}$ should be compared to the surface energy $F_{s\perp} + F_{s\parallel} = 2\pi a^2\sigma_\perp + 4\pi^2\sigma_\parallel ar$ of a cylindrical filament that is a straight circular cylinder of the same cross-sectional radius a and volume as the torus, which means that the length of the cylinder is $2\pi r$. In the straight cylinder, the director is not distorted, thus the elastic energy is 0. The balance of $F_e = 2\pi^2 K_3\left(r - \sqrt{r^2-a^2}\right)$ and $F_{s\perp} = 2\pi a^2\sigma_\perp$ shows that the open-ended cylinder would prefer to curl into toroid, Fig. S2, whenever $\sigma_\perp \ge \frac{\pi K_3 r}{a^2}$. The highest value of K_3 measured in the N phase of DSCG is approximately 50 pN [S12]; with $r \approx 30\ \mu m$, $a \approx 10\ \mu m$, the last condition can be recast as $\sigma_\perp \ge 0.5\times 10^{-4}\ J\ m^{-2}$.

Bend elasticity vs surface tension for complete thin toroids with circular cross-section The ratio of the minor radius to the major radius for thin toroids that are complete and do not touch the substrates is calculated similarly to the main text, as

$$\frac{a}{r} = \left(\frac{V}{2\pi^2}\right)^{\frac{1}{5}}\left(\frac{\sigma_\parallel}{K_3}\right)^{\frac{3}{5}} = \left(\frac{V}{2\pi^2}\right)^{\frac{1}{5}}\frac{1}{\lambda_{ec}^{3/5}} = \frac{1}{2^{1/5}\pi^{2/5}\beta^{3/5}}. \tag{S1}$$

S2. Estimate of the potential range of χ values.

The parameter χ characterizes the relative strength of the surface tension at the glass-LC interface, written as $\chi\sigma_\parallel$, where $\sigma_\parallel$ is the interfacial tension coefficient at the Col-I interface for the columns align parallel to it. The chromonic columns are perpendicular to the glass substrate since tilted alignment would result in a contact of polyaromatic hydrophobic cores of the molecules with water. This alignment and elasticity of the Col phase make the measurements of the surface tension $\chi\sigma_\parallel$ difficult. Below we resort to a simple analytical argument to find the range of plausible values of χ.

Consider a semicircular cylinder of a length L and a radius R attached to the glass by its cross-section of area $2LR$. The elastic energy of bent columns that strike the glass substrate perpendicularly and thus bend over by π, is $\frac{\pi}{2}K_3\ L\ln\frac{R}{r_c}$, where r_c is the radius of the central core. The surface energy of the footprint is $2\chi\sigma_\parallel LR$, the surface energy of the Col-I interfaces is $\pi\sigma_\parallel LR + 2\sigma_\parallel\frac{V}{L}$, where $V = \frac{\pi LR^2}{2}$ =const is the volume of the semicylinder. We use the relationship $V = \frac{\pi LR^2}{2}$ =const to express R through V and L. The surface energy is then $\sqrt{\frac{2VL}{\pi}}(2\chi+\pi)\sigma_\parallel + 2\frac{V}{L}\sigma_\parallel$.

Minimizing the sum of the elastic and surface energies with respect to L, one finds

$$\frac{\pi}{2}K_3\ln\frac{R}{r_c} + \sqrt{\frac{V}{2\pi L}}(2\chi+\pi)\sigma_\parallel - 2\frac{V}{L^2}\sigma_\parallel = 0.$$

For rough estimates, let us represent $V = \frac{\pi LR^2}{2}$ =const as $V = \frac{\pi\xi^2 L^3}{2}$, using a substitution $R = \zeta L$, where $\zeta \sim 1$ is a scaling factor. Since a logarithm is a slow function for large arguments, we treat it as a constant, $\ln\frac{R}{r_c} \approx \ln 50 \approx 4$. Then one finds the equilibrium $L_{eq} = \frac{4\frac{K_3}{\sigma_\parallel}}{2\zeta^2 - \zeta\left(1+\frac{2\chi}{\pi}\right)}$. The last expression could be rewritten as

$$\chi = \frac{\pi}{2}\left(2\zeta - 1 - \frac{4K_3}{\sigma_\parallel\zeta L_{eq}}\right) \tag{S2}$$

In the experiments, nuclei show the shapes that could be roughly characterized by the ratio R/L in the range (0.5 - 1.8). For the typical $L_{eq} \approx 100$ μm, $\frac{K_3}{\sigma_\parallel} = 60$ μm and $\frac{4K_3}{\sigma_\parallel L_{eq}} = 2.4$, the plot $\chi(\zeta)$ suggests that χ might be either positive or negative if the scaling factor is in the plausible range $0.5 \leq \zeta \leq 1.8$, Fig. S3. This conclusion is only qualitative since the experimental shapes with hexagonal footprints are different from the rectangular footprints considered in the model above.

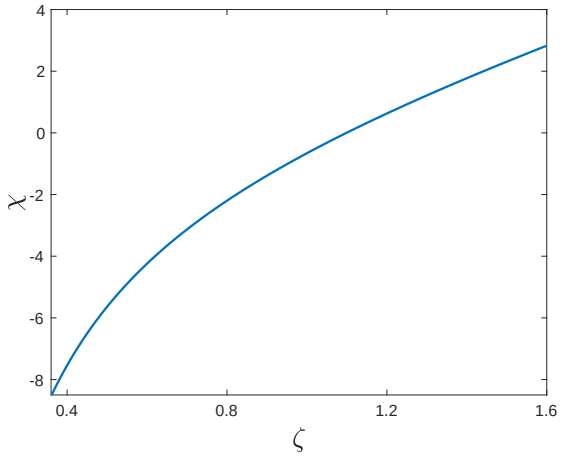

FIGURE S3. Dependence $\chi(\zeta)$ calculated from (S2) for $\frac{4K_3}{\sigma_\parallel L_{eq}} = 2.4$. Note that the parameter χ could be either positive or negative for $0.5 \leq \zeta \leq 1.8$.

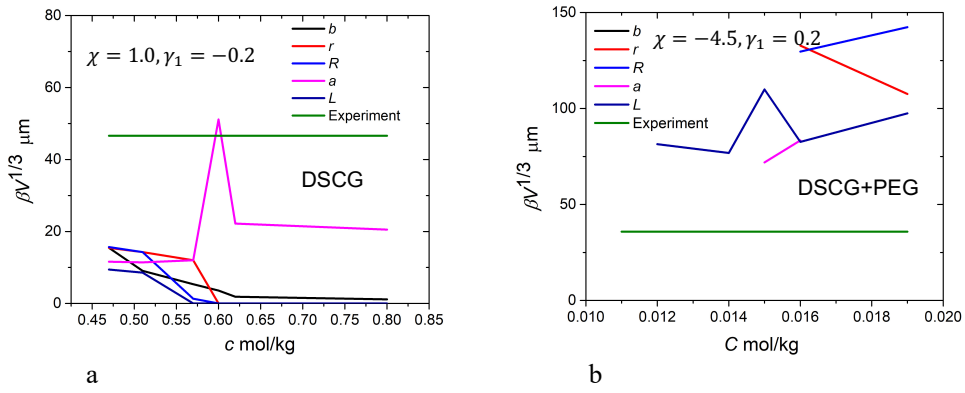

FIGURE S4. Comparison of simulated $\beta V^{1/3}$ to the experimentally obtained values for (a) pure DSCG and (b) DSCG+PEG for parameters that do not match the experimental data: $\chi = 1.0$ and $\gamma_1 = -0.2$ for pure DSCG and $\chi = -4.5$ and $\gamma_1 = 0.2$ for DSCG+PEG.

S3. THERMOMECHANICS OF PLANE CURVES

Here we will follow [S13] to briefly survey the mechanics of a closed plane curve C separating two different phases of a material undergoing a phase transition. Suppose that $\boldsymbol{\nu}$ represents an outward unit normal vector to C and let the line energy density be given by the scalar function $\gamma(\mathbf{x}) = \sigma(\boldsymbol{\nu}(\mathbf{x})) > 0$. The function σ reduces to a positive constant when the line energy is isotropic. Further, let F represent the difference between the bulk energies of the phases.

A positively oriented smooth closed curve is a periodic map $p \Rightarrow \mathbf{r}(p) = (\rho(p), z(p))$ from $\mathbb{R}$ into $\mathbb{R}^2$, such that $|\mathbf{r}'(p)| \neq 0$. Assuming that the curve is positively oriented and parametrized with respect to the arc

length s, we define the orthonormal frame $(\boldsymbol{\tau}(s), \boldsymbol{\nu}(s))$ as

$$\boldsymbol{\tau}(s) = \mathbf{r}'(s) = (\cos\theta(s), \sin\theta(s)), \tag{S3}$$

$$\boldsymbol{\nu}(s) = \mathbf{r}'_{\perp}(s) = (\sin\theta(s), -\cos\theta(s)), \tag{S4}$$

where $\theta(s)$ is the angle between the tangent to the curve and the positive direction of the ρ-axis for all $s \in [0, L]$ and $\mathbf{a}_{\perp} = (a_2, -a_1)$ for every $\mathbf{a} = (a_1, a_2)$. The vectors of the frame are related by the Frenet formulas

$$\boldsymbol{\tau}'(s) = -\kappa(s)\boldsymbol{\nu}(s), \quad \boldsymbol{\nu}'(s) = \kappa(s)\boldsymbol{\tau}(s), \tag{S5}$$

where

$$\kappa(s) = \theta'(s),$$

is the curvature of $\mathbf{r}(s)$. A curve is convex if $\kappa > 0$; this allows to use s and θ as equivalent parameters of the curve. The force sustained by the interface, the capillary force is given by

$$\mathbf{C} = \gamma(\theta)\boldsymbol{\tau} + \gamma'(\theta)\boldsymbol{\nu}. \tag{S6}$$

with a trivial change in notation. For our purposes, we will allow for piecewise smooth curves, that is for $\mathbf{r} = \{\mathbf{r}_1, \mathbf{r}_2, \dots\}$, being a finite or countable collection of continuous arcs, with possibly discontinuous tangent and normal vectors at their junction points.

The concept of stability of the curve with the line energy density γ at a point θ is central in determining the presence of corners and facets on the boundary. Let $\Sigma = \int_{\partial\omega} \gamma\, ds$ denote the total interfacial energy. A necessary and sufficient condition for Σ to have a minimum at θ is that $\gamma(\theta) + \gamma''(\theta) > 0$. The interfacial energy is strictly stable, stable, or unstable at θ provided that

$$\gamma(\theta) + \gamma''(\theta) > 0, \quad \gamma(\theta) + \gamma''(\theta) \geq 0, \quad \gamma(\theta) + \gamma''(\theta) < 0, \tag{S7}$$

respectively. The analogous concepts of global stability or instability follow by requiring the latter to be satisfied for all $\theta \in \mathbb{R}$. When one considers the problem of time evolution of interfaces, instability corresponds to the loss of parabolicity of the governing equation, which becomes backward parabolic at the points of instability of γ.

The construction of the interface curve that minimizes the total line energy is given by Wulff's theorem, stated as follows:

Assume that the difference between the bulk energies of the phases $F \neq 0$. Then

$$\mathbf{r}(\theta) = F^{-1}(\gamma'(\theta)\boldsymbol{\tau}(\theta) - \gamma(\theta)\boldsymbol{\nu}(\theta))$$

defines the interface which is closed, convex and parametrized by θ. Moreover, the curvature is given by

$$\kappa(\theta) = F(\gamma(\theta) + \gamma''(\theta))^{-1}.$$

We now turn to the description of corners and facets observed in experiments. The loss of stability of the function $\gamma(\theta)$ on some θ-intervals can be resolved by allowing corners on the energy minimizing curve $\mathbf{r}(\theta)$. These correspond to jumps in θ across the unstable portions of $\gamma(\theta)$. For a pair of distinct angles $\{\theta^-, \theta^+\}$ to determine an admissible corner, the following conditions must be satisfied: (i) $\gamma(\theta)$ is unstable for $\theta \in (\theta^-, \theta+)$, (ii) $|\theta^+ - \theta^-| < \pi$, and (iii) $\mathbf{C}(\theta^-) = \mathbf{C}(\theta^+)$, representing the continuity of the capillary force at the corner.

The Frank diagram is a central tool to identify corners in the curve. It is the polar diagram of γ^{-1}, and thus the locus of the Frank potential $\boldsymbol{\sigma} = \gamma^{-1}(\theta)\boldsymbol{\nu}(\theta)$. The capillary force is related to the Frank potential in the following way: $\mathbf{C} = -\gamma(\theta)^2\boldsymbol{\sigma}'(\theta)$; it is tangent to the Frank diagram, pointing in the direction of decreasing θ.

The convexity-stability theorem provides an important tool to identify corners: *(i) The Frank diagram is convex if and only if γ is stable. (ii) More generally, γ is stable on the globally-convex sections of the Frank diagram. If (θ^-, θ^+) is an open interval separating two adjacent globally-convex sections, then (θ^-, θ^+) is a corner and γ is unstable somewhere in (θ^-, θ^+).* Hence, the Frank diagram corresponding to a curve with corners has nonconvex regions.

The convexification of the Frank diagram is the polar diagram of a polar function $\Sigma(\theta)$, and hence the locus of a vector potential $\mathbf{\Sigma} = \Sigma(\theta)\boldsymbol{\nu}(\theta)$, the convexified Frank potential. On the globally stable sections of the energy, $\boldsymbol{\sigma}(\theta) = \mathbf{\Sigma}(\theta)$. Between such sections, $\mathbf{\Sigma}$ coincides with the Maxwell lines of the Frank diagram. Consequently, the points of tangency of a Maxwell line with the Frank diagram identify an ordered angular pair corresponding to a corner of the curve (a proper interpretation has to be given to the case that a Maxwell line shares three or more points of tangency with the diagram). Facets correspond to Maxwell lines in the diagram.

S4. Models of Lyotropic Chromonic Liquid Crystals

The simple model that we study assumes that a Col nucleus is composed of circular chromonic "columns" centered on and lying in planes perpendicular to the z-axis. Each cross-section of the nucleus by a plane that contains the z-axis then reveals a triangular lattice of points corresponding to the cross-sections of the columns; we assume that this lattice is fixed with one of the corresponding two-dimensional lattice vectors being parallel to the z-axis. The deformation of the chromonic columns is therefore limited to bending. The bending energy of a given column is proportional to the square of the column curvature as long as we work within the framework of the linear elasticity.

In addition to bending, the total energy also includes the anisotropic surface energy contribution on the boundary between the toroidal aggregate and the surrounding isotropic phase. The equilibrium shape of a toroidal Col nucleus is determined in competition between the surface and the bulk energy contributions. Assuming that the rate of growth of a toroidal aggregate is much slower than the rate at which the balance develops between the surface and the bulk energies, we analyze this balance assuming that the volume of a toroid is fixed.

Given that each toroidal Col nucleus is assumed to be axially symmetric, the geometry of the aggregate is fully determined by its cross-section with a plane that contains the $z-$axis. In order to recover the equilibrium shape of the planar curve that forms the boundary of each cross-section, we will utilize the machinery developed in thermomechanics of plane curves [S14]. Briefly, a curve in [S14] is assumed to represent an interface between two phases with different bulk energies. The equilibrium shape of the curve is dictated by the balance between the bulk energies and the anisotropic line tension within the interface. This is essentially the same situation as we encounter here, except that the bulk energy in our case is spatially-dependent in the columnar phase—this is a principal contribution of the present work. Note that, when a toroid is represented by its cross-section, the surface energy of its boundary reduces to the line energy of the curve bounding the cross-section.

We now postulate the free energy whose minimization gives the optimal shapes of the aggregates in equilibrium. We first introduce the Oseen-Frank energy of nematic liquid crystals as proposed by Oseen, Zocher and Frank,

$$\begin{aligned} W_{\mathrm{OF}} =& \frac{1}{2}K_1(\nabla\cdot\mathbf{n})^2 + \frac{1}{2}K_2(\mathbf{n}\cdot\nabla\times\mathbf{n})^2 + \frac{1}{2}K_3|\mathbf{n}\times\nabla\times\mathbf{n}|^2 \\ &+\frac{1}{2}(K_2+K_4)[(\mathbf{n}\cdot\nabla)\mathbf{n} - (\nabla\cdot\mathbf{n})\mathbf{n})], \quad |\mathbf{n}| = 1, \end{aligned}$$

where the material constants $K_i > 0$, $i = 1, 2, 3$ satisfy Ericksen's inequalities [S15].

The energy of a columnar chromonic liquid crystal consists of the sum of the Oseen-Frank and the transverse elastic energy $\mathcal{W}_{\mathrm{Hex}}$, formulated in terms of the displacement vector $\mathbf{u}$

$$E_h = \int_\Omega W_{\mathrm{OF}}(\mathbf{n}(\mathbf{x}), \nabla\mathbf{n}(\mathbf{x})) + \mathcal{W}_{\mathrm{Hex}}(\nabla\mathbf{u}(\mathbf{x})), \quad \mathbf{n}\cdot\mathbf{u} = 0, \tag{S8}$$

penalizing distortion on planes perpendicular to $\mathbf{n}$. In the expression proposed by de Gennes, [S16],

$$\mathcal{W}_{\mathrm{Hex}} = \frac{1}{2}B\left(u_x + v_y\right)^2 + \frac{1}{2}C\left[\left(u_x - v_y\right)^2 + \left(u_y + v_x\right)^2\right], \quad \mathbf{u} = (u, v). \tag{S9}$$

Note that the total energy includes the elastic free energy of the lattice deformation as well as the bending term of the Oseen-Frank energy, that for small displacements and director distortions, $\delta\mathbf{n}$, can also be expressed in terms of the displacement vector $\mathbf{u}$. The positive constants B and C correspond to compression and shear moduli, respectively. Moreover $B \approx \frac{K_3}{d^2}$, where $d > 0$ represents the typical period of the lattice.

In order to model aggregates of the columnar phase, we assume that the splay K_1 and the twist K_2 elastic constants are much larger than the bending constant K_3, effectively prohibiting both splay and twist deformations. We denote by Ω the domain of a single aggregate with volume $\mathrm{vol}(\Omega) = V$ and with the piecewise smooth boundary $\partial\Omega$. We postulate an anisotropic surface energy density $\sigma_{\|}(\mathbf{x}) = \sigma(\boldsymbol{\nu}(\mathbf{x}), \mathbf{n}(\mathbf{x})))$, where $\boldsymbol{\nu}$ denotes the normal to the boundary $\partial\Omega$ at $\mathbf{x}$. In the current approach, we neglect the elastic energy $\mathcal{W}_{\mathrm{Hex}}$. The free-boundary problem is then formulated as finding the vector field and domain, $(\mathbf{n}, \Omega)$, respectively, that minimize the following energy

$$E[\mathbf{n}] = \frac{K_3}{2}\int_\Omega |\mathbf{n}\times\nabla\times\mathbf{n}|^2\, d\mathbf{x} + \int_{\partial\Omega}\sigma(\boldsymbol{\nu},\mathbf{n})\, ds, \tag{S10}$$

where the admissible director fields $\mathbf{n}$ and sets Ω are subject to the constraints

$$\mathbf{n}\cdot\mathbf{n} = 1, \quad \mathrm{div}\,\mathbf{n} = 0, \quad \mathbf{n}\cdot\mathrm{curl}\,\mathbf{n} = 0 \quad \text{in } \Omega, \tag{S11}$$

$$\boldsymbol{\nu}\cdot\mathbf{n} = 0, \quad \text{on } \partial\Omega, \tag{S12}$$

$$\mathrm{Vol}(\Omega) = V. \tag{S13}$$

Note that the minimization here is performed with respect to both $\mathbf{n}$ and Ω.

As stated, the problem (S10)-(S13) does not include any features of the columnar phase, and thus it can also be used to describe nematic clusters when $K_1, K_2 \gg K_3$.

S5. Derivation of governing equations for smooth curves

Given the energy functional defined in (7), suppose that

$$\partial\omega = \left\{\mathbf{r}(s) = (\rho(s), z(s)) \in \mathbb{R}^2_+ : 0 \le s < L,\ \mathbf{r}(L) = \mathbf{r}(0),\ \mathbf{r}'(L) = \mathbf{r}'(0)\right\},$$

where $L > 0$ and $\mathbf{r}$ is a simple, smooth, positively oriented closed curve parametrized with respect to its arclength. Recall from (S3)-(S4) that $(\boldsymbol{\tau}(s), \boldsymbol{\nu}(s))$ is the orthonormal frame associated with $\mathbf{r}(s)$ and that the curvature of $\mathbf{r}(s)$ at $s \in [0, L]$ is given by $\kappa(s) = \theta'(s)$, where $\theta(s)$ is the angle between the positive direction of the curve and the ρ-axis.

Because we are interested in optimizing the shape of $\partial\omega$, we consider variations $\delta\mathbf{r}$ of $\mathbf{r}$ of the form $\delta\mathbf{r} = (\delta f)\boldsymbol{\nu}$ where $\delta f : [0, L] \to \mathbb{R}$ satisfy $\delta f(0) = \delta f(L)$ and $\delta f'(0) = \delta f'(L)$. The variations of the first and the last integrals are then given by

$$\delta\left(2\beta\int_\omega \rho^{-1} dA\right) = 2\beta\int_{\partial\omega}\rho^{-1}\delta f\, ds = 2\beta\int_0^L \rho(s)^{-1}\delta f(s)\, ds \tag{S14}$$

and

$$\delta\left(4\lambda\int_\omega \rho\, dA\right) = 4\lambda\int_{\partial\omega}\rho\,\delta f\, ds = 4\lambda\int_0^L \rho(s)\delta f(s)\, ds, \tag{S15}$$

respectively. At the same time

$$\delta\left(2\int_{\partial\omega}\sigma(\boldsymbol{\nu})\rho\, ds\right) = 2\int_0^L \left\{\nabla\sigma(\boldsymbol{\nu}(s))\cdot\delta\boldsymbol{\nu}(s)\rho(s) + \sigma(\boldsymbol{\nu}(s))\delta\rho(s) + \sigma(\boldsymbol{\nu}(s))\rho(s)\boldsymbol{\tau}(s)\cdot\delta\mathbf{r}'(s)\right\} ds. \tag{S16}$$

Note that

$$\delta\mathbf{r}'(s) = \delta f'(s)\boldsymbol{\nu}(s) + \delta f(s)\kappa(s)\boldsymbol{\tau}(s)$$

and

$$\delta\boldsymbol{\nu}(s) = -\delta f'(s)\boldsymbol{\tau}(s).$$

Substituting these expressions into (S16) and integrating by parts, we obtain

$$\delta\left(2\int_{\partial\omega}\sigma(\boldsymbol{\nu})\rho\,ds\right)=2\int_0^L\left\{\left[\rho(s)\nabla\sigma(\boldsymbol{\nu}(s))\cdot\boldsymbol{\tau}(s)\right]_s+\sigma(\boldsymbol{\nu}(s))\left(\mathbf{e}_\rho\cdot\boldsymbol{\nu}(s)+\rho(s)\kappa(s)\right)\right\}\delta f(s)\,ds, \tag{S17}$$

where $\mathbf{e}_\rho=(1,0)$. Now, combining (S14), (S15), and (S17) and omitting the s-dependence, we find that the Euler-Lagrange equation satisfied by a critical point of the energy (7) is

$$\left[\rho\nabla\sigma(\boldsymbol{\nu})\cdot\boldsymbol{\tau}\right]_s+\sigma(\boldsymbol{\nu})\left(\mathbf{e}_\rho\cdot\boldsymbol{\nu}+\rho\kappa\right)+\frac{\beta}{\rho}-2\lambda\rho=0. \tag{S18}$$

If we recall (S3)-(S4) and set

$$\gamma(\theta):=\sigma\left(\sin\theta,-\cos\theta\right),$$

then it is immediately follows that

$$\gamma_\theta=\nabla\sigma(\boldsymbol{\nu})\cdot\boldsymbol{\tau}.$$

Using this expression and (S3)-(S5) in (S18) gives an alternative form of the Euler-Lagrange equation

$$\rho\kappa\left(\gamma_{\theta\theta}+\gamma\right)+\gamma\sin\theta+\gamma_\theta\cos\theta+\frac{\beta}{\rho}-2\lambda\rho=0. \tag{S19}$$

Combining the equations obtained in this section, we determine the full problem for the unknown (ρ,θ,z,L) satisfied by the energy-minimizing curve. The problem is given by the system of ODEs

$$\begin{cases}\rho\left(\gamma_{\theta\theta}+\gamma\right)\theta'+\gamma\sin\theta+\gamma_\theta\cos\theta+\frac{\beta}{\rho}-2\lambda\rho=0,\\ \rho'=\cos\theta,\\ z'=\sin\theta,\end{cases} \tag{S20}$$

subject to the conditions

$$\theta(L)=\theta(0)+2\pi,\quad \theta'(L)=\theta'(0),\quad \int_0^L\cos\theta\,ds=\int_0^L\sin\theta\,ds=0,\quad 2\pi\int_\omega\rho\,dA=1. \tag{S21}$$

Using the second equation in (S20) we observe that

$$\rho'\left(\rho\left(\gamma_{\theta\theta}+\gamma\right)\theta'+\gamma\sin\theta+\gamma_\theta\cos\theta\right)=\left(\rho\gamma_\theta\cos\theta+\rho\gamma\sin\theta\right)'.$$

We proceed by multiplying the first equation in (S20) by ρ' and integrating with respect to s to obtain

$$\rho\left(\gamma_\theta\cos\theta+\gamma\sin\theta\right)+\beta\log\rho-\lambda\rho^2=\mathcal{D} \tag{S22}$$

on $[0,L]$ where $\mathcal{D}$ is a constant. The equation (S22) provides the relationship between the ρ-coordinate of a point on the curve $\partial\omega$ and the angle between $\partial\omega$ and the ρ-axis at the same point. An immediate consequence of (S22) is that flat facets on $\partial\omega$ may be present only if they are parallel to the z-axis, when ρ on these facets remains constant.

Although in the preceding discussion we assumed that the energy-minimizing curve is smooth, it is possible that this curve will develop corners where the curvature is not defined and the angle function θ is not differentiable. To this end, observe that the only term in (7) where the derivative of θ would appear following integration by parts is the surface energy term. We can adapt our variational argument in order to handle this situation as demonstrated in the main text of the paper.

S6. Analysis

From now on, we suppose that $\gamma:\mathbb{R}\to\mathbb{R}$ is a smooth, 2π-periodic and strictly positive function. Borrowing once again from [S13], we have that (i) the Frank diagram associated with γ is convex as long as $\gamma_{\theta\theta}+\gamma>0$ for all $\theta\in[0,2\pi)$ and the energy minimizing curve $\mathbf{r}$ cannot have corners; (ii) if the Frank diagram is not convex, then the curve $\mathbf{r}$ has corners, but not cusps. The angles at which corners occur for a given γ are fixed by the corresponding Frank diagram and are well-separated if the Maxwell lines of a given diagram have no common points (regular diagram in the terminology of [S13]).

We look for a convex, piecewise-smooth curve $\mathbf{r}$ that solves (S20)-(S21). If $\gamma_{\theta\theta}+\gamma$ is not strictly positive on $[0,2\pi)$, we impose an additional technical assumption on γ that it achieves a local minimum at some $\theta_0 \in (0,\pi)$.

Lemma 1. *The Lagrange multiplier λ is strictly positive.*

Proof. Since $\mathbf{r}$ is convex, $\theta' \geq 0$ away from the corners. If $\gamma_{\theta\theta}+\gamma$ is strictly positive on $[0,2\pi)$, then there are no corners and the result immediately follows by evaluating (S20) at $\pi/2$. Otherwise, θ_0 is not inside a corner and $\gamma_{\theta\theta}(\theta_0)+\gamma(\theta_0) > 0$ hence $\lambda > 0$ by evaluating (S20) at θ_0. □

Next, observe that the jump condition (12) implies that $\gamma_\theta \cos\theta + \gamma \sin\theta$ is continuous across the corners. Due to continuity of $\mathbf{r}$ we then have that (S22) holds even when $\mathbf{r}$ has corners.

With Lemma 1 in mind, we introduce the rescaling

$$\tilde{\rho} = \lambda\rho,\ \tilde{z} = \lambda z,\ \tilde{s} = \lambda s,\ \tilde{L} = \lambda L,\ \tilde{\beta} = \lambda\beta$$

then, dropping tildes for notational convenience and taking advantage of (S22), we can rewrite the problem (S20)-(S21) in the form

$$\text{(S23)} \qquad \begin{cases} \rho\,(\gamma_{\theta\theta}+\gamma)\,\theta' + \gamma\sin\theta + \gamma_\theta\cos\theta + \dfrac{\beta}{\rho} - 2\rho = 0, \\ \rho\,(\gamma_\theta\cos\theta + \gamma\sin\theta) + \beta\log\rho - \rho^2 = \mathcal{D}, \\ z' = \sin\theta \end{cases}$$

for $s \in [0,L]$, subject to the conditions

$$\text{(S24)} \qquad \theta(L) = \theta(0) + 2\pi, \quad \theta'(L) = \theta'(0), \quad \int_0^L \sin\theta\, ds = 0$$

and (12) at the corners whenever discontinuities of θ are present. Note that we can drop the condition $\int_0^L \cos\theta\, ds = 0$ and the volume constraint in (S21) because periodicity of ρ is ensured by the first equation in (S23) and the volume constraint can be satisfied by an appropriate rescaling, respectively. In addition to the functions ρ, z, and θ, the unknowns of the problem (S23)-(S24) also include the constants $\mathcal{D}$ and L.

S6.1. **Analysis of the model for curves without corners.**

Assume that $\gamma_{\theta\theta}+\gamma$ is strictly positive on $[0,2\pi)$ so that the energy minimizing curve is smooth. As long as this curve is also convex, we have that

$$\min_{s\in[0,L]} \rho(s) = \rho\left(-\frac{\pi}{2}\right) \text{ and } \max_{s\in[0,L]} \rho(s) = \rho\left(\frac{\pi}{2}\right).$$

Let

$$\rho_m := \rho\left(-\frac{\pi}{2}\right) \text{ and } \rho_M := \rho\left(\frac{\pi}{2}\right)$$

and suppose that

$$h(\theta) := \gamma_\theta\cos\theta + \gamma\sin\theta.$$

The following claim holds.

Claim 1. *The function h is strictly increasing from*

$$h_m := h\left(-\frac{\pi}{2}\right) = -\gamma\left(-\frac{\pi}{2}\right)$$

to

$$h_M := h\left(\frac{\pi}{2}\right) = \gamma\left(\frac{\pi}{2}\right)$$

when $\theta \in \left(-\frac{\pi}{2},\frac{\pi}{2}\right)$, while it is strictly decreasing from h_M to h_m when $\theta \in \left(\frac{\pi}{2},\frac{3\pi}{2}\right)$.

Proof. The claim immediately follows from

$$(\gamma_\theta\cos\theta + \gamma\sin\theta)_\theta = (\gamma_{\theta\theta}+\gamma)\cos\theta,$$

along with 2π-periodicity of γ and positivity of $\gamma_{\theta\theta}+\gamma$. □

With the help of Claim 1, we conclude that there exist unique $\theta_+ \in \left[-\frac{\pi}{2}, \frac{\pi}{2}\right]$ and $\theta_- \in \left[\frac{\pi}{2}, \frac{3\pi}{2}\right]$ such that $h(\theta_-) = h(\theta_+) = 0$. Now, fix a constant $a > 0$ and set $\rho(\theta_-) = a$. Then, the second equation in (S23) can be written as

$$h\rho + \beta \log \rho - \rho^2 = \beta \log a - a^2, \tag{S25}$$

for every $\theta \in [0, 2\pi]$.

Claim 2. *Let a_* be the positive solution of*

$$h_m t_* + \beta \log t_* - t_*^2 = \beta \log a_* - a_*^2, \tag{S26}$$

where

$$t_* = \frac{\sqrt{h_m^2 + 8\beta} + h_m}{4}.$$

For every $a > a_*$ and $h \in [h_m, h_M]$, there is a unique solution $\varrho(h, a) > a$ of (S25) *that continuously increases with h. For $a < a_*$, no such solution of* (S25) *exists.*

Proof. Consider two functions

$$\phi(t) = h_m t + \beta \log t - t^2$$

and

$$\psi(t) = \beta \log t - t^2$$

when $t > 0$. Then

$$\phi(t) < \psi(t)$$

for every $t > 0$ because $h_m < 0$ and (S25) at $\theta = -\frac{\pi}{2}$ can be written in the form

$$\phi(\rho_m) = \psi(a),$$

where $\rho_m < a$. Further, the function ϕ and ψ both have a single maximum and no minima when $t > 0$ and the maximum of ϕ is at

$$t_* = \frac{\sqrt{h_m^2 + 8\beta} + h_m}{4}.$$

It follows that the equation $\phi(\rho_m) = \psi(a)$ can only be satisfied if $\psi(a) \le \phi(t_*)$. When combined with the condition $\rho_m < a$, it is easy to see that this will be true when $a > a_*$ with a_* defined in the statement of the claim (cf. Fig. S5). It is also easy to see that, as long as the equation (S25) can be solved at h_m, it can also

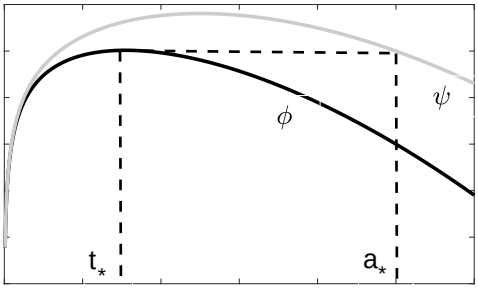

FIGURE S5. Choice of t_* and a_*.

be solved for every $h > h_m$. Indeed, rewriting the equation (S25) again, now as

$$h\rho = \rho^2 - a^2 - \beta \log \rho/a, \tag{S27}$$

we observe that the graphs of the functions of ρ on the right and left sides of (S25) intersect at the point $(\rho_m, \rho_m h_m)$. As h increases from h_m to h_M, the slope of the linear function on the left side of (S27) increases. The function on the right of (S25) is independent of h, it has a single minimum on $\mathbb{R}_+$, and it goes to infinity when $\rho \to 0^+$ or $\rho \to \infty$. We conclude that, as h monotonically increases from h_m to h_M, the equation (S27)

has two continuous solution branches: one monotonically increasing and another monotonically decreasing with h. Since the solution curve $\mathbf{r}$ that we seek is convex, we select $\varrho(h, a)$ from the branch along which ρ increases with h. □

Note that the function ϱ is independent of the surface energy density γ and the surface energy is only used in Claim 2 to describe the range of h. The solution $\rho_a(\theta)$ of the second equation in (S23) with $\rho_- = a$ and parametrized with respect to θ is then given by

$$\rho_a(\theta) = \varrho(h(\theta), a).$$

Observe that exactly the same solution branch will be traversed by $\rho(h(\theta), a)$ in opposite directions as θ varies between $\left[-\frac{\pi}{2}, \frac{\pi}{2}\right]$ and $\left[\frac{\pi}{2}, \frac{3\pi}{2}\right]$, respectively. Further, it follows that $\rho_+ = \rho_-$.

The remainder of the solution procedure can be significantly simplified if the curve is strictly convex, because it can be parametrized with respect to θ instead of s. With a slight abuse of notation, the reparametrization $(\rho(\theta), z(\theta))$ solves

$$\text{(S28)} \qquad \begin{cases} h\rho + \beta \log \rho - \rho^2 = \beta \log a - a^2, \\ z' = \dfrac{\rho^2 \left(\gamma_{\theta\theta} + \gamma\right) \sin\theta}{2\rho^2 - h\rho - \beta}, \end{cases}$$

when $\theta \in [0, 2\pi]$ along with a condition that $z(0) = z(2\pi)$.

We can now outline a possible procedure for finding a solution of (S23)–(S24) corresponding to a strictly convex curve $\mathbf{r}$. Choose $a > 0$ and, for every $h \in \left[h\left(-\frac{\pi}{2}\right), h\left(\frac{\pi}{2}\right)\right]$, determine $\varrho(h, a)$ as outlined in Claim 2. The function $\rho_a(\theta) = \varrho(h(\theta), a)$ solves the second equation in (S23). The function $z_a(\theta)$ can then be determined by integrating already known expression on the right hand side of the second equation in (S28). In order to satisfy the constraint $z(0) = z(2\pi)$ we must have

$$\text{(S29)} \qquad \int_0^{2\pi} \frac{\rho_a^2(\theta) \left(\gamma_{\theta\theta}(\theta) + \gamma(\theta)\right) \sin\theta}{2\rho_a^2(\theta) - h(\theta)\rho_a(\theta) - \beta} \, d\theta = 0,$$

and this can be ensured by iterating in a.

As we will show below, however, the existence of a strictly convex minimizing curve is not guaranteed even in the case of an isotropic surface energy because the curve may develop vertical facets when β is sufficiently small. Indeed, it is possible that there is no $a > a_*$ such that (S29) holds. In that case, and as long as $z(2\pi) - z(0) > 0$, the following modification to the solution can be made. Set $a = a_*$ so that $\rho_m = t_*$ according to (S29). Because t_* is a critical point of the function ϕ in the proof of Claim 2, we have

$$h_m \rho_m + \beta \log \rho_m - \rho_m^2 = 0,$$

then the curvature

$$\theta'\left(-\frac{\pi}{2}\right) = 0,$$

according to the first equation in (S23). The solution curve then can be closed in a smooth way by completing it with a straight vertical facet. This procedure is illustrated in the next section, where we numerically solve the algebraic equations derived above assuming that the surface energy density is isotropic.

S6.2. **Numerical results for isotropic surface energy.**

In this section we set $\gamma \equiv 1$ so that $h(\theta) = \sin\theta$. We solved (S23) in MATLAB using the iterative process described at the end of the previous section. The results are illustrated below in Figs. S6-S9. All computations in the remainder of this paper are done in nondimensional variables and, in particular, assuming that the volume of the toroid is equal 1.

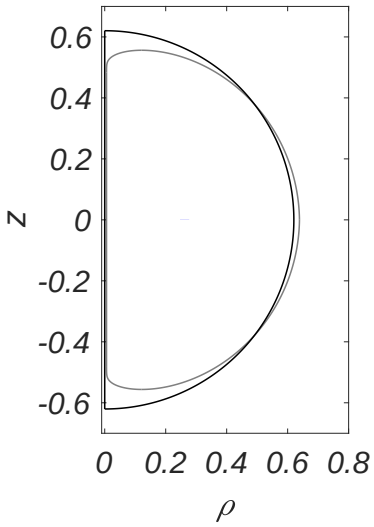

FIGURE S6. Comparison between the shapes of cross-sections of a toroid with $\beta = 0.006$ and the limiting half-disk corresponding to the sphere of the same volume as the toroid.

Note that, if $\beta = 0$, there is no contribution from the bending energy and the variational problem reduces to minimizing the surface area of the axially symmetric three-dimensional region subject to a volume constraint. In this case the energy-minimizing domain Ω has the shape of a sphere and, hence, ω becomes a half of a disk. In turn, we expect that for a small $\beta > 0$ the shape of a minimizing curve will be close to that of a half of a circle where the endpoints of the arc are connected by the diameter. Indeed, this is what can be observed in Fig. S6 for $\beta = 0.006$.

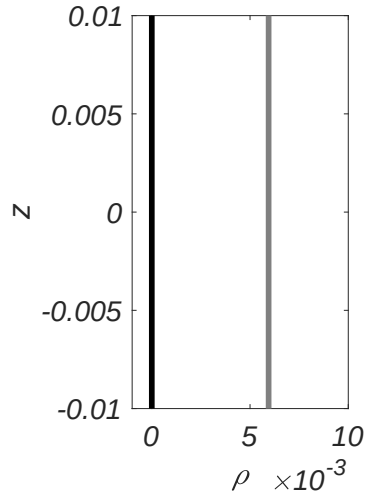

FIGURE S7. The same setup as in Figure S6, zoomed in at z-axis. Note that the facet (grey line) is indeed at the distance comparable to β from the axis as indicated by (S30).

Because the cost of bending diverges as the curve approaches z-axis, we also expect that the energy-minimizing curve should remain separate from that axis, with the distance decreasing as β becomes smaller. Here an expansion of t_* with respect to a small β leads to the following estimate

$$d := \operatorname{dist}(\partial\omega, \{\rho = 0\}) \sim \beta \tag{S30}$$

for the distance between the curve and the z-axis in the isotropic case. Fig. S7, corresponding to the configuration depicted in Fig. S6 zoomed in near the origin, confirms this estimate.

As β gets larger, bending becomes more expensive in comparison with the surface energy—even away from the z-axis—and the size of the toroidal domain should increase with β. At the same time, the diameter of a cross-section of the torus by a plane containing the z-axis should decrease with β increasing while the shape of this cross-section approaches that of a disk. This behavior can be seen in Fig. S8.

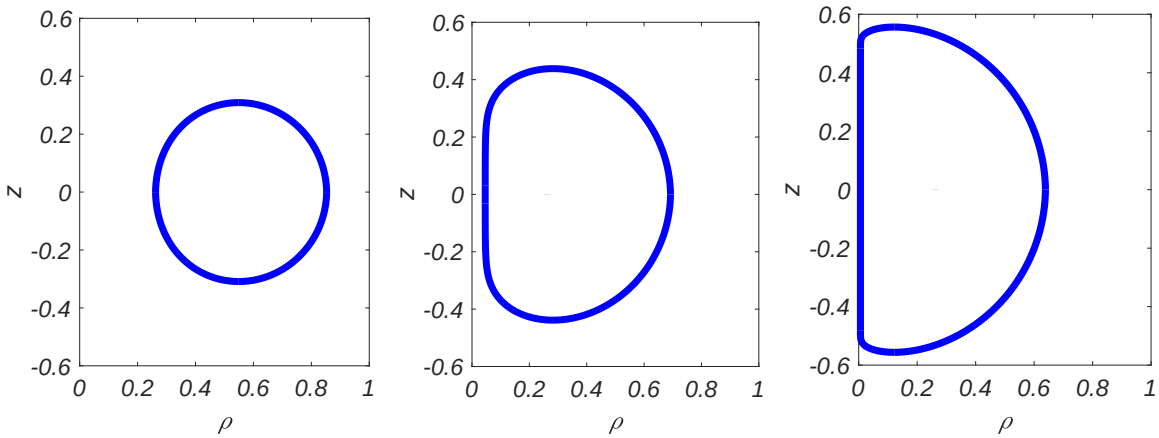

FIGURE S8. Cross-sections of the energy-minimizing toroids for the isotropic surface energy: $\beta = 0.006$ (right), $\beta = 0.054$ (middle), $\beta = 0.41$ (left).

When β is small, we observed that there is a critical value of β, below which $\rho_{min} = t_*$ defined in Claim 2. As it was discussed at the end of Section S6.1, this indicates that a vertical facet forms on the side of the torus that faces the z-axis; this facet increases in length when $\beta \to 0$ as shown in Fig. S9.

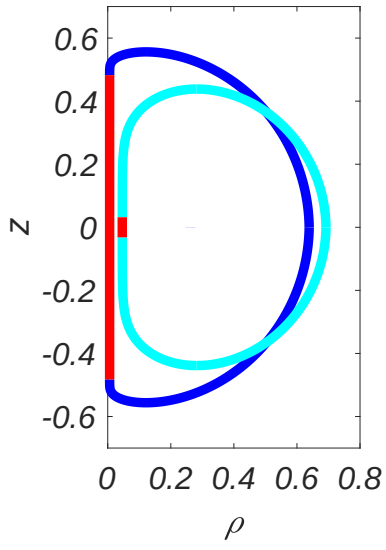

FIGURE S9. Cross-sections of toroids with vertical facets for the isotropic surface energy (facets are indicated in red). From left to right: $\beta = 0.006$ (blue), $\beta = 0.054$ (cyan).

Finally, we compared the solutions obtained by using the iterative procedure for solving (S23) with the solutions obtained via the gradient flow. The comparison for $\beta = 0.054$ and $\gamma \equiv 1$ is shown in Fig. S10.

Here the gradient flow simulations were done assuming that the regularization parameter $\varepsilon = 0$ because the surface energy is isotropic. Fig. S10 shows a good match between the predictions of the two methods.

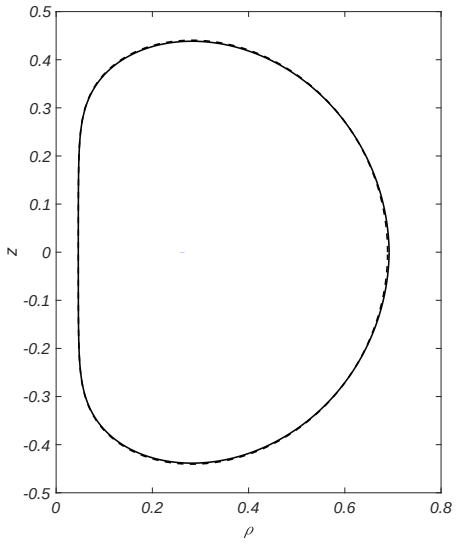

FIGURE S10. Comparison between the solutions of the system (S23) (solid line) vs the minimizer found via gradient flow with $\varepsilon = 0$ (dashed line). Here $\beta = 0.054$ and we assume that the surface energy is isotropic.

S6.3. **Numerical results for weakly anisotropic surface energies.**

We simulate curves with anisotropic surface energy by setting

$$\gamma(\theta) = 1 + \gamma_1 \sin^2(3\theta) \tag{S31}$$

First, we consider the case when $\gamma_1 = -0.03$. The Frank diagram, Wulff plot, and Wulff construction corresponding to this choice of surface energy are shown in Fig. S11. Observe that the Frank diagram in this case is strictly convex and the Wulff construction predicts a configuration with six rounded facets and no sharp corners. This is indeed a shape of the cross-section of the torus that we obtained in simulations in Fig. S12 (right) for the same γ_1 and a relatively large value of β. For such beta, similar to the results in the isotropic case, the major radius r of the torus is large while its minor radius a is small in order to accommodate significant bending energy and the volume constraint. Because $a/r \ll 1$, the variation of ρ across the cross-section is smaller than ρ itself and the weight ρ in the integral corresponding to the capillary force can be considered to be essentially constant. As the result, the shape of the cross-section is close to that obtained via the Wulff construction. On the other hand, increasing K_3 and β or decreasing $\sigma_{\|}$ and volume, expands the central narrow core into a wider "donut hole" (Fig. S12). We also observe that the corners and facets become more rounded with decreasing β and the parts of the curve closest to the z-axis transform into a facet.

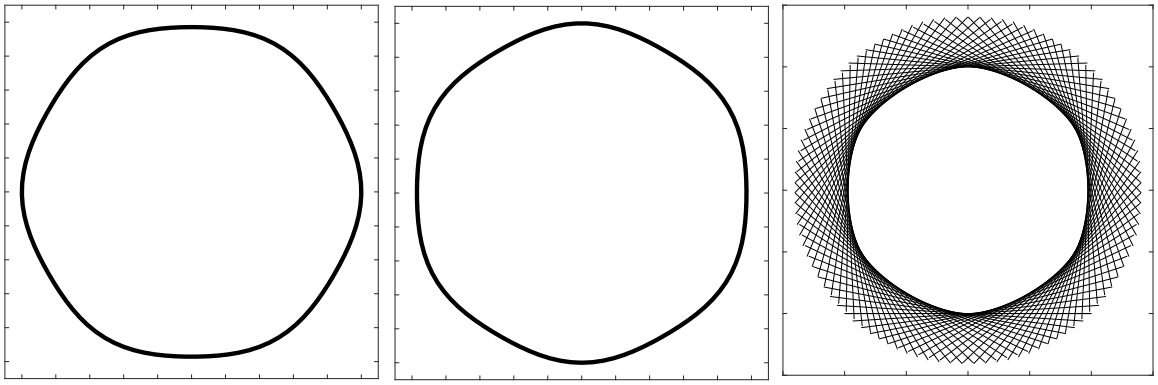

FIGURE S11. Frank diagram (left), Wulff plot (middle), and Wulff construction for the anisotropic surface energy $\gamma(\theta) = 1 + \gamma_1 \sin^2(3\theta)$ with $\gamma_1 = -0.03$.

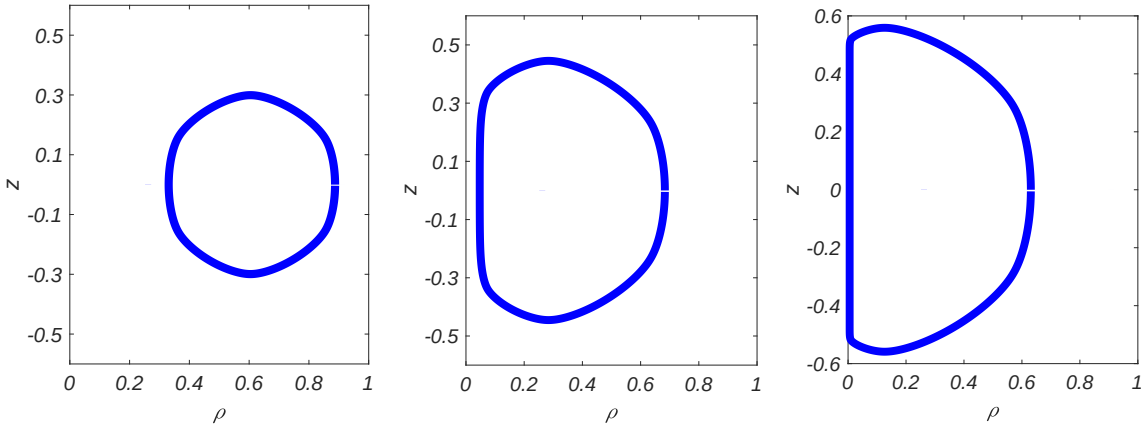

FIGURE S12. Cross-sections of the energy-minimizing toroids for the anisotropic surface energy $\gamma(\theta) = 1 + \gamma_1 \sin^2(3\theta)$ with $\gamma_1 = -0.03$ and $\varepsilon = 0$. Here $\beta = 0.54$ (left), $\beta = 0.054$ (middle), and $\beta = 0.0054$ (right).

Enchancing the surface anchoring to $\gamma_1 = -0.1$ (See Fig. S13 for the corresponding Frank diagram, Wulff plot, and Wulff construction) does not change the situation significantly (Fig. S14): for the same small $\beta = 0.0054$, the part of the crystal closest to the z-axis is essentially similar to that for $\gamma = -0.03$. However, away from the axis, faceting becomes more pronounced and is similar to the shape observed for the corresponding Wulff construction Fig. S13. Note that, in this case, the Frank diagram is no longer convex and there are six Maxwell lines that indicate that the equilibrium shape must have six corners. The corners in Fig. S14 are rounded due to regularization employed in the gradient flow simulations (this regularization is not needed when the Wulff construction has a smooth shape).

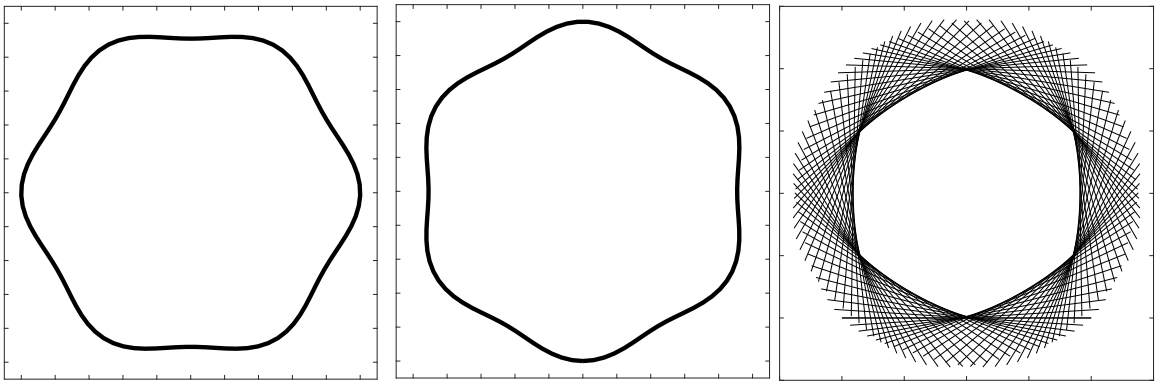

FIGURE S13. Frank diagram (left), Wulff plot (middle), and Wulff construction for the anisotropic surface energy $\gamma(\theta) = 1 + \gamma_1 \sin^2(3\theta)$ with $\gamma_1 = -0.1$.

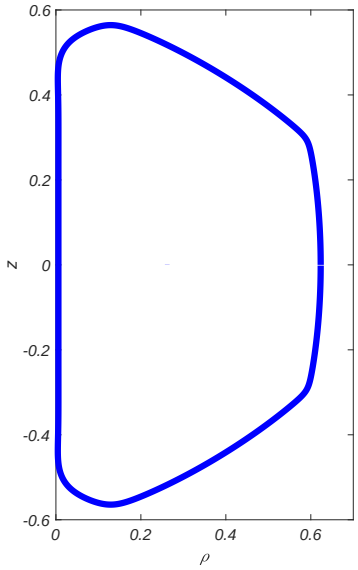

FIGURE S14. Cross-sections of the energy-minimizing toroid for the anisotropic surface energy $\gamma(\theta) = 1 + \gamma_1 \sin^2(3\theta)$ with $\gamma_1 = -0.1$, $\varepsilon = 10^{-4}$, and $\beta = 0.0054$.

REFERENCES

[S1] L. Sallen, P. Oswald, J.C. Géminard, and J. Malthête, "Surface tension and elasticity of hexagonal columnar mesophases," *J. Phys. II France*, vol. 5, no. 7, pp. 937–961, 1995.

[S2] M. E. Glicksman and K. Ankit, "Measuring solid–liquid interfacial energy fields: diffusion-limited patterns," *Journal of Materials Science*, vol. 53, no. 15, pp. 10955–10978, 2018.

[S3] H. Princen, I. Zia, and S. Mason, "Measurement of interfacial tension from the shape of a rotating drop," *Journal of Colloid and Interface Science*, vol. 23, no. 1, pp. 99–107, 1967.

[S4] G. Vliegenthart and H. Lekkerkerker, "Measurement of the interfacial tension of demixed colloid-polymer suspensions," *Trends in Colloid and Interface Science XI*, pp. 27–30, 1997.

[S5] E. H. de Hoog and H. N. Lekkerkerker, "Measurement of the interfacial tension of a phase-separated colloid- polymer suspension," *The Journal of Physical Chemistry B*, vol. 103, no. 25, pp. 5274–5279, 1999.

[S6] M. M. Villone and H. A. Stone, "Rotating tensiometer for the measurement of the elastic modulus of deformable particles," *Phys. Rev. Fluids*, vol. 5, p. 083606, Aug 2020.

[S7] S. Zhou, K. Neupane, Y. A. Nastishin, A. R. Baldwin, S. V. Shiyanovskii, O. D. Lavrentovich, and S. Sprunt, "Elasticity, viscosity, and orientational fluctuations of a lyotropic chromonic nematic liquid crystal disodium cromoglycate," *Soft Matter*, vol. 10, pp. 6571–6581, 2014.

[S8] S. Zhou, Y. A. Nastishin, M. M. Omelchenko, L. Tortora, V. G. Nazarenko, O. P. Boiko, T. Ostapenko, T. Hu, C. C. Almasan, S. N. Sprunt, J. T. Gleeson, and O. D. Lavrentovich, "Elasticity of lyotropic chromonic liquid crystals probed by director reorientation in a magnetic field," *Phys. Rev. Lett.*, vol. 109, p. 037801, Jul 2012.

[S9] S. Zhou, A. J. Cervenka, and O. D. Lavrentovich, "Ionic-content dependence of viscoelasticity of the lyotropic chromonic liquid crystal sunset yellow," *Phys. Rev. E*, vol. 90, p. 042505, Oct 2014.

[S10] H.-S. Park, S.-W. Kang, L. Tortora, Y. Nastishin, D. Finotello, S. Kumar, and O. D. Lavrentovich, "Self-assembly of lyotropic chromonic liquid crystal sunset yellow and effects of ionic additives," *The Journal of Physical Chemistry B*, vol. 112, no. 51, pp. 16307–16319, 2008.

[S11] M. Kleman and O. D. Laverntovich, *Soft matter physics: an introduction*. New York: Springer-Verlag, 2003.

[S12] S. Zhou, *Elasticity, Viscosity, and Orientational Fluctuations of a Lyotropic Chromonic Nematic Liquid Crystal Disodium Cromoglycate*, pp. 51–75. Cham: Springer International Publishing, 2017.

[S13] S. Angenent and M. E. Gurtin, "Multiphase thermomechanics with interfacial structure. 2. Evolution of an isothermal interface," *Archive for Rational Mechanics and Analysis*, vol. 108, pp. 323–391, Nov 1989.

[S14] S. Angenent and M. E. Gurtin, "Multiphase thermomechanics with interfacial structure. 2. evolution of an isothermal interface," in *Fundamental Contributions to the Continuum Theory of Evolving Phase Interfaces in Solids: A Collection of Reprints of 14 Seminal Papers* (J. M. Ball, D. Kinderlehrer, P. Podio-Guidugli, and M. Slemrod, eds.), pp. 196–264, Berlin, Heidelberg: Springer Berlin Heidelberg, 1999.

[S15] E. G. Virga, *Variational Theories for Liquid Crystals*, vol. 8. Chapman and Hall, London, 1st ed., 1994.

[S16] P. G. de Gennes and J. Prost, *The Physics of Liquid Crystals*. Oxford: Clarendon Press, 1993.

Advanced Materials and Liquid Crystal Institute, Materials Science Graduate Program, Kent State University, Kent, OH 44242, USA

Email address: rkoizumi@kent.edu

Department of Mathematics, The University of Akron, Akron, OH 44325-4002

Email address: dmitry@uakron.edu

Advanced Materials and Liquid Crystal Institute, Department of Physics, Kent State University, Kent, OH 44242, USA and Department of Physics, University of Bisha, Bisha, 67714, Saudi Arabia

Email address: aalqarn1@kent.edu

Department of Mathematics, Louisiana State University, Baton Rouge, LA 70803-4918

Email address: walker@lsu.edu

Advanced Materials and Liquid Crystal Institute, Kent State University, Kent, OH 44242, USA and Hetman Petro Sahaidachnyi National Army Academy, 32 Heroes of Maidan street, Lviv, 79012, Ukraine

Email address: nastyshyn_yuriy@yahoo.com

School of Mathematics, University of Minnesota, Minneapolis, MN 55455, USA

Email address: calde014@umn.edu

Advanced Materials and Liquid Crystal Institute, Materials Science Graduate Program, Kent State University, Kent, OH 44242, USA and Department of Physics, Kent State University, Kent, Ohio 44242, USA

Email address: olavrent@kent.edu